“Urban biomining meets printable electronics: end-to-end at destination biological recycling and reprinting”

NNH17ZOA001N, NIAC Phase 1 report

3 February 2017

Lynn J. Rothschild (PI)

Jessica Koehne, Ram Gandhiraman, Co-Is;

Jesica Navarrete, Ph.D. student

Dylan Spangle, Masters student

Phase I Abstract

Space missions rely utterly on metallic components, from the spacecraft to electronics. Yet, metals add mass, and electronics have the additional problem of a limited lifespan. Thus, current mission architectures must compensate for replacement. In space, spent electronics are discarded; on earth, there is some recycling but current processes are toxic and environmentally hazardous. Imagine instead an end-to-end recycling of spent electronics at low mass, low cost, room temperature, and in a non-toxic manner. Here, we propose a solution that will not only enhance mission success by decreasing upmass and providing a fresh supply of electronics, but in addition has immediate applications to a serious environmental issue on the Earth. Spent electronics will be used as feedstock to make fresh electronic components, a process we will accomplish with so-called "urban biomining" using synthetically enhanced microbes to bind metals with elemental specificity. To create new electronics, the microbes will be used as "bioink" to print a new IC chip, using plasma jet electronics printing. The plasma jet electronics printing technology will have the potential to use martian atmospheric gas to print and to tailor the electronic and chemical properties of the materials. Our preliminary results have suggested that this process also serves as a purification step to enhance the proportion of metals in the "bioink". The presence of electric field and plasma can ensure printing in microgravity environment while also providing material morphology and electronic structure tunabiity and thus optimization. Here we propose to increase the TRL level of the concept by engineering microbes to dissolve the siliceous matrix in the IC, extract copper from a mixture of metals, and use the microbes as feedstock to print interconnects using mars gas simulant. To assess the ability of this concept to influence mission architecture, we will do an analysis of the infrastructure required to execute this concept on Mars, and additional opportunities it could offer mission design from the biological and printing technologies. In addition, we will do an analysis of the impact of this technology for terrestrial applications addressing in particular environmental concerns and availability of metals.

1. Table of Contents

2. Introduction

2.1 The Problem

Advances in 3D printing allow for the manufacture of objects with materials such as plastics and metals. NASA needs next generation manufacturing technologies to embed structural electronics into objects built at destination. For integrated circuits (IC chips) for example, traditional photolithography patterning and multi-layer deposition are neither amenable for non-planar substrates nor affordable for installation on Mars. Manufacturing technologies that could work in reduced to microgravity are needed to print electronics in space. To date, there is no single printing technology available for in-space manufacturing that can print IC chips or passive electronic components on non-conventional substrates (i.e., non-silicon). Precise control over thickness and material properties are required, and with minimal processing steps. The other key challenge is the acquisition of the feedstock materials. Possible sources are Earth, in situ resource utilization, or the recycling of spent electronics. The last two require technologies that are toxic, heavy and expensive. Currently, metals are extracted from solution using step-wise processes such as through high temperature smelting, chemical precipitation and/or electroplating.

2.2 The Vision

Integrated circuitry has revolutionized modern technology by allowing for faster and smaller processors through the use of metals doped into a silicon wafer. Printed electronics have the potential to revolutionize electronics manufacturing and allow for flexible electronic devices on non-traditional substrates. While relatively inexpensive on the Earth, a supply in space must be regenerated, repurposed or repaired in situ. IC chips are a crucial part of many electronic devices, however, their manufacture requires pure substrates that require extensive processing to obtain.[1] The microelectronics industry relies on well-established combination of photolithography, deposition and etching.[1] State-of -the-art processes are not amenable for three dimensional or non-planar substrates and are bulky.[1] Revolutionary manufacturing technologies, that can challenge conventional electronics fabrication and enable embedding of micro/nano-electronics on non-planar, non-silicon based substrates, are needed. Our vision is to use synthetic biology to reduce an IC chip into individual elemental components and to use these substrates to re-print electronic components using our plasma jet electronics printer with Martian atmospheric gases with low toxicity, mass and expense. Thus, our vision is no less than a synthetic biology-enabled smart manufacturing tool that uses the

Martian atmosphere to tailor material properties. Near term, we envision enabling printing on location on ISS as well as offering a solution to the increasing environmental issue of recycling spent electronics on Earth.

2.3 The Concept

The overall objective of this work is to take the first steps towards an end-to-end IC chip recycling and reprinting facility on Mars, using the power of biology to reduce mass, toxic waste and high heat requirements, while immediate use is envisioned for Earth and ISS. Here we will develop the biotechnology to reduce an IC chip to its elemental components, in the form of a "bioink", using genetic engineering. We have developed a novel manufacturing tool that uses an atmospheric pressure plasma jet for printing.[2,3] This technology will be used to print the elemental materials that are mined using engineered microorganisms (the "bioink"). This plasma printer has the potential to use Martian atmospheric gases to generate the plasma. Ultimately, an integrated in-space/*in situ* manufacturing facility with integrated electronics capability will be a means to obtain or repair complex electronics without requiring an extensive manufacturing facility.

Initially, an obsolete IC chip will serve as the starting material to be separated into its elemental components with enzymatic and metal-binding systems developed through synthetic biology. Silicon dioxide (SiO_2), an insulator, will be obtained by using silicase enzymes to depolymerize the silicate matrix of the IC chip and then silicatein enzymes will be used to re-assemble the necessary SiO_2. These enzymes are derived from bacteria that prey on diatoms. Bacteria will be engineered to bind specific metals to their flagella by inserting metal-binding motifs in the flagellin protein subunits, thus allowing them to be expressed external to the cell and in large quantity. The bacteria will be used as metal "inks." During the plasma printing process the cells are destroyed removing concerns about biological contamination and thus planetary protection issues with the finished product. The cells that would be handled prior to printing would be the common and benign soil a bacterium, *Bacillus subtilis*. This species is ideal for NASA as it forms extremely resistant spores that have been shown to survive for several years in space, and is safe for astronauts to handle.[4,5]

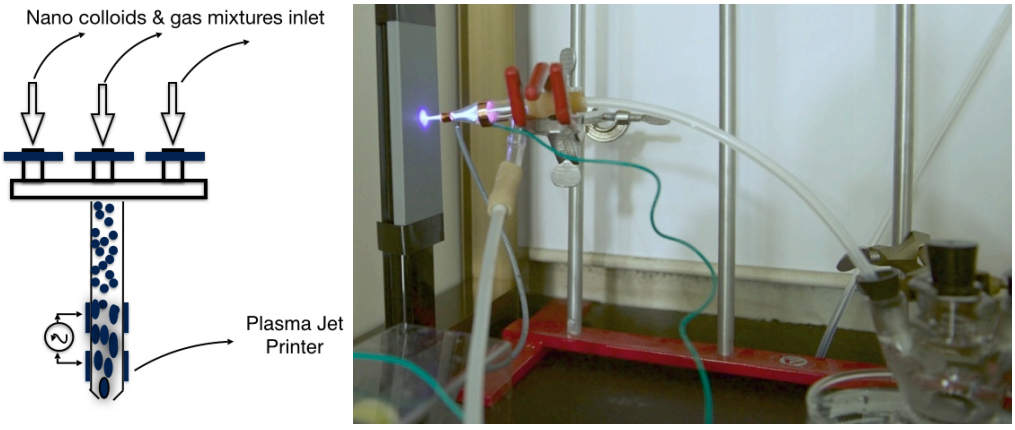

Figure 1. (left) Schematic of plasma jet printer with provision for multiple inputs (right) Photograph of plasma jet printer and plasma jet directly and with further processing (e.g., metal extraction) as needed to produce functional ICs. In Phase I we proposed using a bioink.

The plasma jet printer shown in Figure 1 consists of a dielectric nozzle and two metal electrodes connected to a high voltage power supply for creating a plasma discharge. Aerosolized ink is pushed out of the nozzle by a carrier gas and is further focused by the plasma to create fine printed features. The electron density of a plasma discharge varies depending on the properties of the gas used to generate the plasma. At atmospheric pressure, the electron density of argon plasma is 2.5 times that of the helium plasma.[6] As a result, the current density and the deposition temperature varies. The thermal conductivity of the gases is different, and thus the deposition temperature varies. The material properties, including oxidation state and electronic conductivity will be tailored using a novel *in situ* printing process. By using an appropriate choice of gas mixtures to include reactive gases like O_2, N_2, H_2, CO_2, and non-reactive gases such as argon, the material properties can be tailored. Depending on the need, either single jet and/or multiple jets could be used for printing conductor, semiconductor and insulator.

This technology can lower energy and materials requirements, and decrease toxicity and environmental impact for IC production significantly by using low temperature, biological techniques to generate the feedstock for the IC chips or by editing of an existing IC chip.

2.4 Innovation

Biomining: In an IC chip, layers of conductive metals (Cu, Au, Pt) alternate between layers of insulating silica (SiO_2). To recycle the metals contained within integrated circuits, the SiO_2 insulating layers must be removed. This can be accomplished by heating the silicate to its melting temperature of between 1400-3900 °C (depending on

the metal-dopant), or dissolving it with hydrofluoric acid so that the metallic components separate from the silicate matrix. Our innovation is to use a bioengineered silicase enzyme to dissolve the silica matrix and to then separate the different elemental components in an IC chip using proteins that bind specific metals. This is a novel approach to recycling the materials in glass- and metal-containing e-waste. Our approach separates complex chemical mixtures into elemental components at ambient pressures and temperatures without the need for energy intensive, high temperature redox chemical separation. Our innovation is a low-energy, passive recovery of materials for recycling and re-use through the novel use of bacterial surfaces for selectively binding metals in a solution.

Printing: Atmospheric pressure plasma jet printing is simple and easy to construct with very low volume and weight. It allows for printing electronics on non-planar, non-traditional objects using biologically-acquired electronic materials. The material properties of the deposited materials can be tailored *in situ* and printing using Martian atmospheric gas is possible. Application of an electric field at the print nozzle and the presence of plasma jet provides directionality for printing in a micro-gravity environment. Ability to deposit conductive patterns, insulators, dielectric materials, and semiconductors using a single printing tool, is a sophistication that is not available with any other printing technology.

2.5 Benefits

2.5.1 Concept for NASA

- Enables in-space manufacturing and repair of critical electronic components for future Mars and current ISS missions using the power of biology, *in situ* resources and plasma jet printing.
- An easy to construct, low mass and volume smart manufacturing tool that can be used in micro gravity with a sterile product eliminating planetary protection concerns.
- Recycling of spent metals in orbit on at destination, and extraction of metals from planetary basalts.

2.5.2 Concept for nation: Commercial potential

- Recovery of metals in a non-toxic, low cost, room temperature manner. Critical as sources of rare earth metals are increasingly constrained for geopolitical and environmental reasons.

- Advanced manufacturing technology that is amenable to 3D and non-planar substrates. An attractive feature for flexible electronics and 3D printed electronics.
- *In situ* tailoring of material properties in printed electronics is a unique characteristic of plasma jet printing that is not feasible with any other printing technology.
- There is currently no infrastructure in place for the efficient recovery of metals from e-waste. Recycling of resources would minimize the environmental impacts from mining for metals.

2.5.3 This study

- Initial instrumentation design for microgravity, further bioink optimization and removal of silicate matrix for mission concept.
- Analysis of use and implementation of technology for Mars mission, ISS and on Earth.
- Training for Ph.D. student and master's student; outreach potential. Development of "green technology."

3. Results of Phase I

3.1 Objective 1. Increase the technical TRL level of the concept.

To increase the TRL to at least 2, we tackled several of the greatest unknowns in achieving this vision, the specificity of metal binding to engineered bacteria, dissolving the siliceous matrix, printing with a simulation of Mars atmospheric gases, and using the new bioinks for printing.

3.1.1. Depolymerization of silica

Increase the extraction of metals by mixing a ground IC with genetically engineered bacteria to de-polymerize the silica in the chip. This same approach will be necessary for extracting metals from basalts.

3.1.1.1 Background

In an IC, layers of conductive metals (Cu, Au, Pt) alternate between layers of insulating silica (SiO_2). To recycle the metals contained within integrated circuits, the SiO_2 insulating layers must be removed. This can be accomplished by heating the silicate to its melting temperature of between 1400-3900 °C (depending on the metal-dopant), or

dissolving it with hydrofluoric acid so that the metallic components separate from the silicate matrix. Our innovation is to use a bioengineered silicase enzyme to dissolve the silica matrix and to then separate the different elemental components in an IC chip using proteins that bind specific metals. This is a novel approach to recycling the materials in glass- and metal-containing e-waste. Our approach separates complex chemical mixtures into elemental components at ambient pressures and temperatures without the need for energy intensive, high temperature redox chemical separation. Our innovation is a low-energy, passive recovery of materials for recycling and re-use through the novel use of bacterial surfaces for selectively binding metals in a solution.

The objective of this phase of our project is to increase the TRL of the technology. By demonstrating positive results in proof-of-concept experiments, we argue that the depolymerization of silica has reached TRL 3, "Analytical and experimental critical function and/or characteristic proof of concept." We have successfully produced *E. coli* cultures that are genetically modified to express silicase from the thermophilic archeon *Methanosarcina thermophila*. Robust expression of the protein has been experimentally shown using SDS-PAGE with a LumioTM fluorescent identification tag. We have shown dissolution of SiO_2 from glass beads incubated with the soluble protein fraction containing silicase, using the silicomolybdic acid spectrophotometric method. We have tentatively determined optimal environmental conditions for further silica degradation assays. Experiments to build on these findings and determine the rate of SiO_2 depolymerization are now underway.

3.1.1.2 Procedure

Gene construct: A polymerase chain reaction (PCR) was performed to amplify a pUC19 vector using silicase-end-specific primers, in order to prepare for insertion of the *M. thermophila* silicase gene into the vector for use in *E. coli* transformation. In addition to containing the silicase gene, the vector was designed to contain an ampicillin resistance marker (for selection purposes), a 6x histidine tag and a tetracysteine tag (Figure 2.) The His tag allows the translated protein to be targeted specifically for elution by Ni-NTA purification, while the Cys tag creates a binding site for the Lumio™ Green fluorescent detection reagent. After amplification, the DNA solution was run on an agarose gel at 123 V for 37 minutes, and the 3 kb band was extracted from the gel using a GenCatch™ DNA gel extraction kit (Epoch Life Sciences, Missouri City, TX) and protocol. The

concentration of the extracted DNA was measured using NanoDrop spectrophotometry at 260 nm wavelength, and showed approximate DNA concentrations of 20-25 ng/µL.

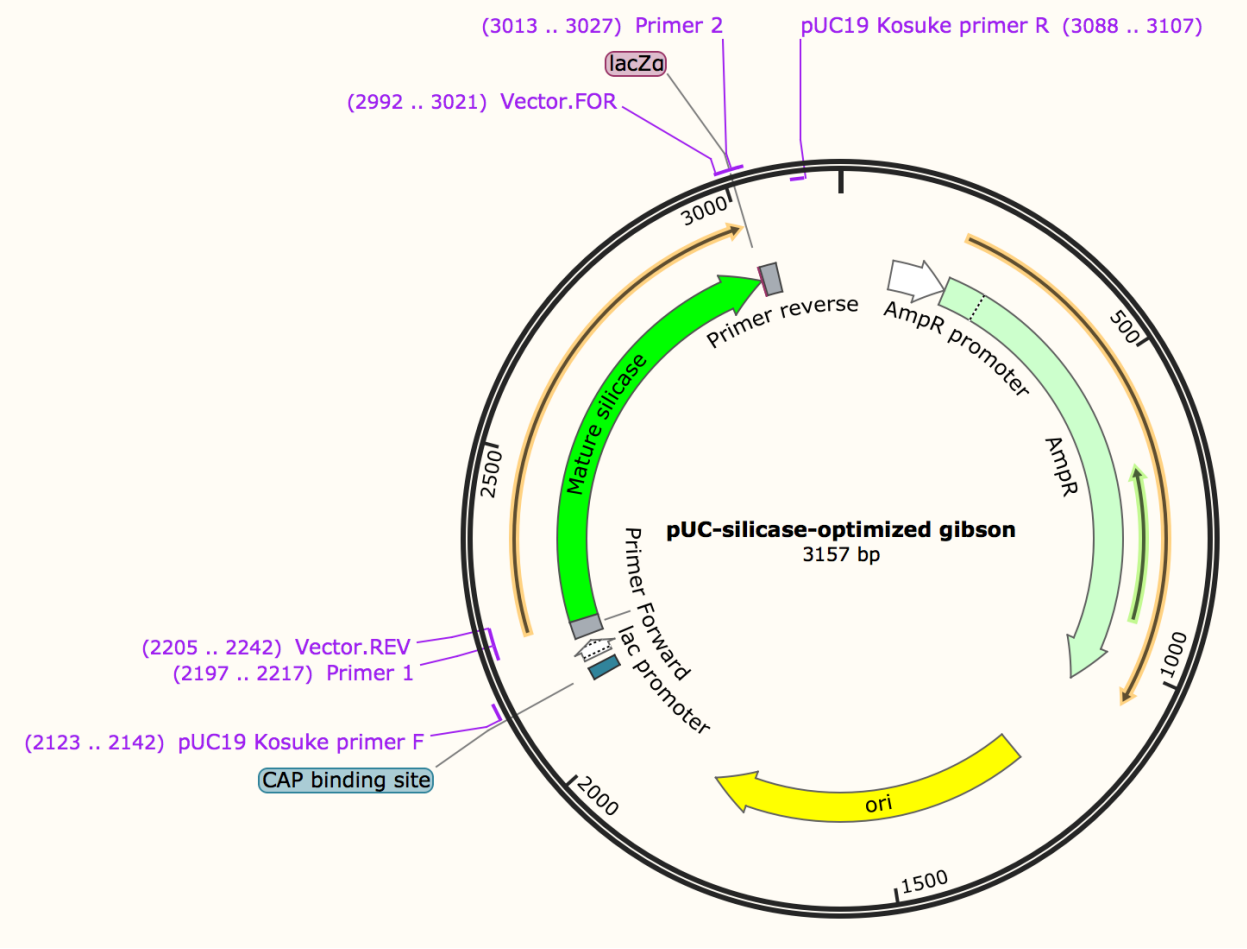

Fig 2. Planned vector as seen in SnapGene software. The 6xHis and tetracysteine tags (mentioned above) not shown.

Using Gibson assembly master mix (New England Biolabs, Ipswich, MA), the *M. thermophila* silicase gene fragment was inserted into the modified vector as shown in Figures 2 and 3.

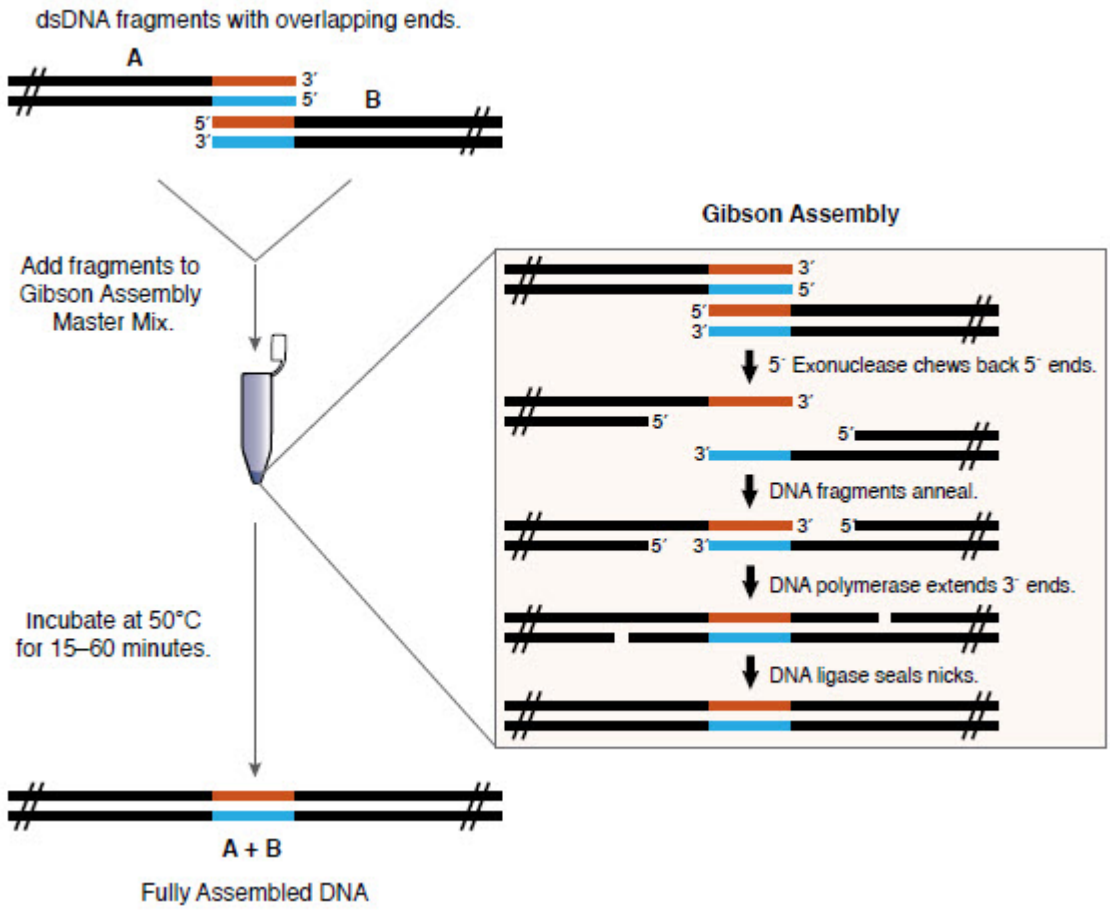

Fig 3. Gibson Assembly method summary.

The resulting product was transformed into *E. coli* cells of two strains: T7 Express and NEB-5-Alpha, both sourced from New England Biolabs. Because of their genotypes, T7 are preferred for protein expression, while the NEB strain is typically used for maintaining plasmids. Two µL of the Gibson assembly mix were added to the *E. coli* stocks, and were transformed according to manufacturer directions.

Three colonies were sampled from each transformed plate culture and grown in 5 mL LB+ampicillin (200 µg/mL) cultures at 37˚C for 2-3 hours. The resulting cultures were centrifuged and the cell pellet collected and analyzed for protein production. One µL was taken from each culture and the silicase gene was amplified to detectable levels by PCR, in order to verify the sequence did not contain insertions or deletions. To probe for protein production, we analyzed the soluble and insoluble fractions using CelLyticB (Sigma) and Inclusion Body Reagent (Sigma-Aldrich, St. Louis, MO), respectively. Lumio™ green reagent was added to 15 µL of each protein fraction and analyzed on SDS-PAGE and analyzed for fluorescence at 488_{ex} and 526_{em} nm light. Fluorescence was

detected in all soluble fraction samples, indicating the presence of silicase protein with the tetracysteine tag.

Fig. 4. SDS-PAGE gel with Lumio fluorescence signified by dark bands.

The 5 mL starter cultures were added to 2 L of LB medium with ampicillin for large-scale culture and protein extraction. Soluble protein extract was collected and 200 µL of 64 mM $ZnCl_2$ was added to provide Zn cofactor for silicase activity.

Silicase activity assays:

Soluble protein extract was incubated with 0.1 mm diameter glass beads. They were separated into four groups with different conditions of temperature and either shaking or stationary. Control experiments were carried out with water in place of soluble protein fraction.

A: 25˚ shaking
B: 25˚ non-shaking
C: 37˚ shaking
D: 37˚ non-shaking

Each group contained four tubes of control (H_2O) and experimental sample (soluble protein extract) separated by ratio to glass beads, either 3:4 or 9:10.

Silicase was purified from the soluble protein extract using Thermo Fisher Ni-NTA resin, which the 6x His tag binds to specifically. This was done according to the normal product guidelines. Flow-through fractions were stored at 4 ˚C in preparation for SDS-PAGE analysis and a BCA assay. SDS-PAGE was performed to determine presence of silicase in purified protein fractions (Lumio) as well as contamination with other proteins (SYPRO Orange stain). The BCA assay results showed a protein concentration of about 50 µg/mL in the purified protein solution.

Heteropoly Blue (silicomolybdic acid spectrophotometric method) assay: quantifying silica dissolution in soluble protein fraction from T7 silicase transformant.

Plate design (Table 1).

Silica standard was diluted 1000 ppm (+/- 5) in gradient on rows A and B (each row was duplicate of the other). Due to cross-contamination, standard dilutions were repeated on rows G and H.

	1	2	3	4	5	6	7	8
A	1000 ppm standard	750 ppm standard	500 ppm standard	250 ppm standard	100 ppm standard	50 ppm standard	25 ppm standard	0 ppm standard
B	1000 ppm standard	750 ppm standard	500 ppm standard	250 ppm standard	100 ppm standard	50 ppm standard	25 ppm standard	0 ppm standard
C	Ab3/4	Ap3/4	Ab9/10	Ap9/10				
D	Bb3/4	Bp3/4	Bb9/10	Bp9/10				
E	Cb3/4	Cp3/4	Cb9/10	Cp9/10				
F	Db3/4	Dp3/4	Db9/10	Dp9/10				
G	1000 ppm standard	750 ppm standard	500 ppm standard	250 ppm standard	100 ppm standard	50 ppm standard	25 ppm standard	0 ppm standard
H	1000 ppm standard	750 ppm standard	500 ppm standard	250 ppm standard	100 ppm standard	50 ppm standard	25 ppm standard	0 ppm standard

Table I. Silica test plate design.

Each well was filled with a sequence of 4 µL molybdate 3 reagent, citric acid F reagent, and amino acid F reagent from the HACH Heteropoly Blue kit. Silica and phosphate in the sample react with molybdate ions under acidic conditions to form yellow silicomolybdic acid complexes and phosphomolybdic acid complexes. The addition of citric acid destroys the phosphate complexes. Amino Acid F Reagent was then added to reduce the yellow silicomolybdic acid to an intense blue color, which is proportional to the silica concentration. The plate was then read at 815 nm.

Results of this assay showed significant dissolution of silica where protein was present, compared to controls containing water (Table 2). Shaking did not appear to be necessary to maximize silica dissolution, and room temperature appeared sufficient.

	1:4 silica to protein	1:4 silica to water	1:10 silica to protein	1:10 silica to water
25°C with shaking	827.88	197.01	339.71	91.83
25°C no shaking	781.19	153.76	703.36	88.73
37°C with shaking	793.78	26.60	714.60	100.08
37°C no shaking	773.86	344.71	739.58	29.42

Table II. Results of silicase incubation with glass beads.

Fig. 5. Results of first Heteropoly Blue assay, measuring silica dissolution after four days of incubation. Concentrations listed are in mg/L. Results suspected of being influenced by error marked in red on table.

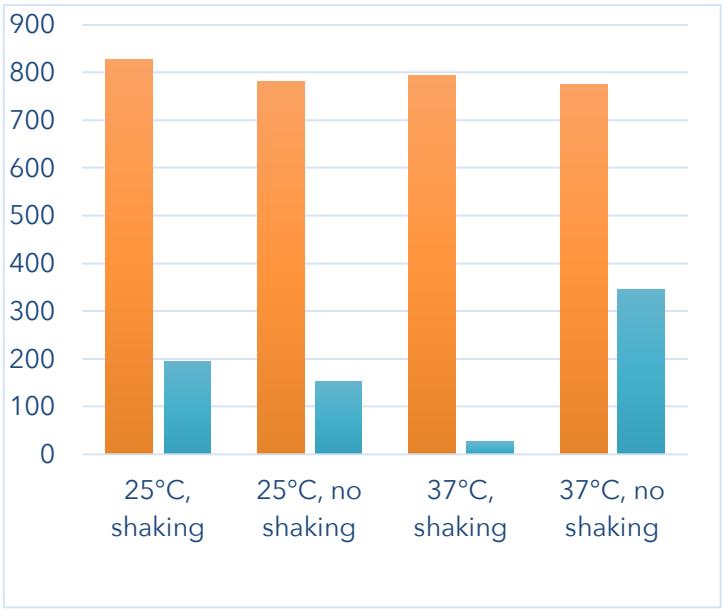

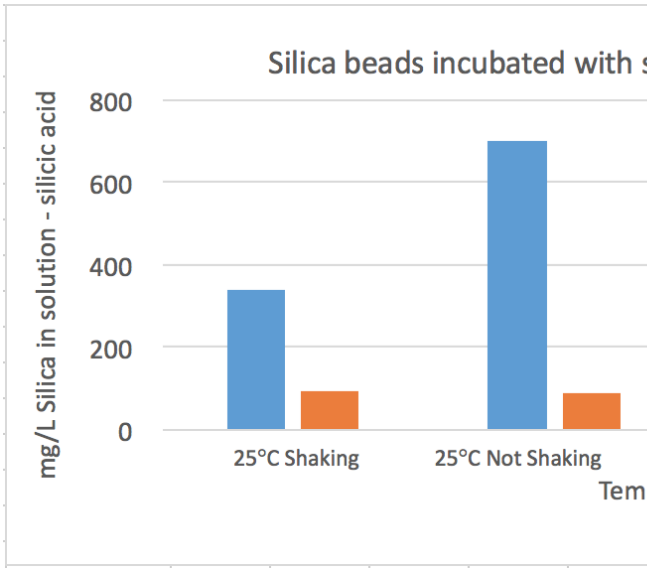

Imaging of glass beads before and after incubation in soluble protein extract showed notable pitting.

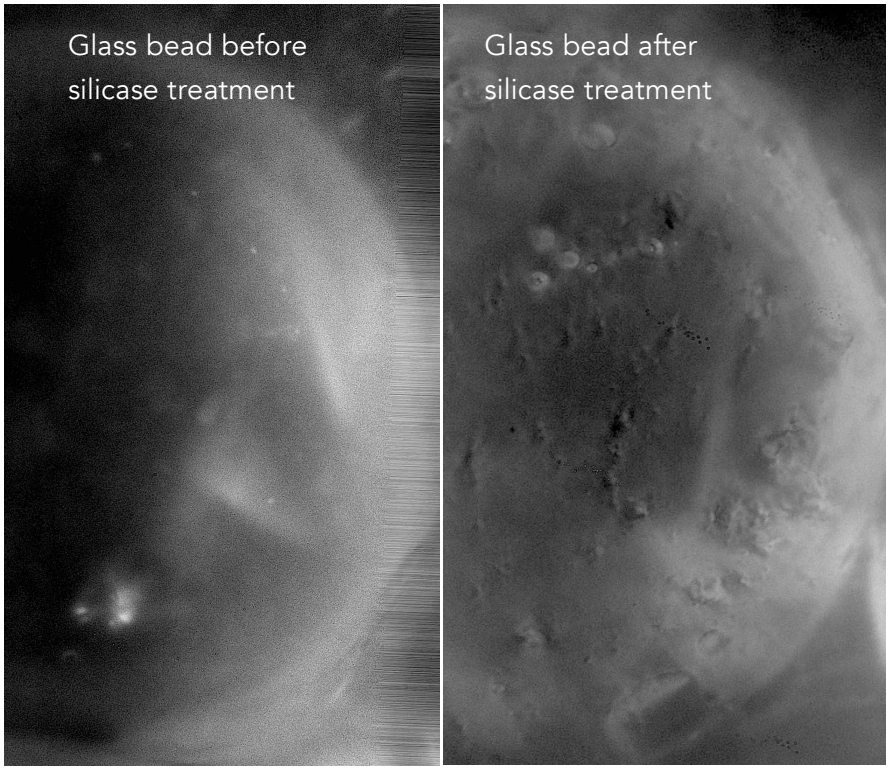

Fig. 6. Glass beads before and after treatment with silicase. Silicase treatment has produced visual pitting in the surface. Stacked Images taken with Canon EOS 60D Macropod Pro Micro Kit (Macroscopic Solutions, Tolland, CT)

We performed a second Heteropoly Blue assay using purified silicase. The samples were incubated at 25˚C without shaking, since that did not appear to have a significant effect on the outcome in the previous experiment. We incubated 0.33 g of 0.1 mm glass beads in purified silicase, as well as in TBS buffer

without silicase to act as a control. We also incubated purified silicase without *any* silica to see if the protein was being stained by the Heteropoly Blue assay, and thus interfering with results. Results showed no staining of protein, suggesting that we can trust our earlier results to accurately represent silica dissolution in the soluble protein fraction. However, the results of this second assay showed a lack of significant silica dissolution by purified silicase.

Fig. 7. Selected results from second Heteropoly Blue assay with purified silicase

It has been hypothesized that the Zn in the soluble protein fraction was washed out during Ni-NTA purification, robbing the silicase of an important co-factor. Our next experiments will involve re-adding Zn after the purification step.

Conclusions: Transgenic silicase is very effective at dissolving silica beads and thus is promising for dissolving the silica matric of an IC or a basalt.

3.1.2 Copper binding by bacteria

Assess the metal-binding specificity of the copper-binding bacterial construct by starting with a solution of copper and then adding additional metals found in an IC.

To increase the TRL to at least 2, we addressed several unknowns by testing the specificity of metal binding to engineered bacterial surfaces and using the metal-enriched biomass for plasma printing with a simulation of Mars atmospheric gases.

3.1.2.1 Rationale

After enzymatic degradation of the silicate matrix, the metals remain in solution. Copper is universally used in IC chips and electronics but often exists in a mixture with other metals after the matrix is removed. Currently, metals are extracted from solution using step-wise processes such as through high temperature smelting, chemical precipitation and/or electroplating. Biohydrometallurgy is an emerging biotechnology where microbial processes are used to sequester or recover metal ions from aqueous solutions. Biological (green) technologies to reclaim metals will serve to ease our dependence on foreign mines and there are economic benefits as biologically-mediated extraction lowers cost of metal recovery when compared to traditional extraction methods.

We proposed a biological approach to metals separation and since the chemistry and role of Cu in metalloproteins is relatively well-characterized, we used Cu as a proxy to elucidate metal and biological ligand interactions with various metals in e-waste. We assessed the binding parameters of three representative classes of Cu-binding motifs using isothermal titration calorimetry: 1) natural motifs found in metalloproteins, 2) consensus motifs, and 3) rationally designed peptides that are predicted, *in silico*, to bind Cu. Many of the metals contained in e-waste, however, have no role in biology, thus no natural binding partners exist. *Our approach is to use Cu as a representative to elucidate on the key determinants of metal specificity and to apply these principles to other metals of economic interest with no known biological function, such as rare-earth or platinum group elements.* Here, we present the results from our initial studies that focus on the specificity of metal-binding motifs for a cognate metal. The candidate motifs that show high affinity and specificity will be engineered into bacterial surfaces for downstream applications in biologically-mediated metal recycling.

Since our target metals exist in an aqueous solution with competing ligands that affect how available a metal is to its corresponding ligand, the fidelity of a construct to its cognate metal (Cu) was assessed in competition assays with competing metals. We used isothermal titration calorimetry to determine which of our peptide constructs are most efficient at binding Cu under conditions with competing ions. Our aims were to assess proteins for specificity and binding parameters such as binding affinity (Ka), enthalpy (ΔH) and entropy ($T\Delta S$).

3.1.2.2 Methods

Peptide synthesis and reagents

Peptides were synthesized by Elim Biopharmaceuticals (Hayward, CA), purified by HPLC with (H)Cl as the counter ion and provided as a lyophilized powder. Purity was >98% and verified through mass-spectrometry. Peptides were modified to have N-terminal acetylation and C-terminal amidation to avoid having a charged peptide. Concentrations for the reconstituted peptides were determined by Pierce™ BCA Assay.

The peptides assessed for binding parameters are listed in Table III.

Type	Name	Amino Acid Sequence	Cognate metal	Source
Natural motifs	HypB1	CTTCGCG	Unknown	Fu et al., 1995 [7]
	HypB2	MCTTCGCGEG	Unknown	Chung et al., 2008 [8]
	CZB-7	GFHGRADALLHKI	Cu/Zn	Yeh et al., 2010 [9]
Consensus	Cu-02	HCWCHM	Cu	Bertini et al., 2010 [10]
Rational design	HHTC	HNLGMNHDLQGERPYVTEGC	Cu	Kozisek et al., 2008 [11]
	CHSK	CPSEDHVSQDK	Cu	
	KDTK	KTEYVDERSKSLTVDLTK	Zn	
	KDKD	KFFKDFRHKPATELTHED	Zn	
	TSMQ	TLSRGSTEDQMDIVGFSQEEQ	Cd	

Table III. Candidate peptide motifs.

The buffer chosen for the ITC experiments was 10 mM, 2-(N-morpholino)-ethanesulfonic acid (MES) buffer. It was chosen because it has been shown to not cause metal ion interference because of complexation or amine oxidation, is stable through the entire range of pH 3-11, and has a stable pK_a over a relatively wide temperature range (15°C – 45°C).[12,13] Buffer pH for peptides and metal solutions was 5.5 to prevent metals precipitating into solid mineral phases. Metal chloride salts were used as the source of metal ions, and speciation was verified through thermodynamic modeling using Visual Minteq 3.0.[14] Concentrations for metal stock solutions were determined through ICP-OES at the University of California Santa Cruz, Center for Earth and Marine Sciences.

Determination of binding parameters

Isothermal titration calorimetry (ITC) was used to determine the association equilibrium constant (K_a), enthalpy (ΔH), and the number of ions bound per ligand (n). A review of ITC theory is thoroughly described in Nielsen et al., 2003.[15] The association equilibrium constant, K_a, is a value that often determines the affinity of a ligand for its substrate and ITC is widely used to determine binding affinities for metal ions to proteins.[16] The instrument used to obtain measurements was a Malvern MicroCal iTC200 (http://www.malvern.com/en/products/product-range/microcal-range/microcal-itc-range/microcal-itc200/) in the Space Biosciences Division at NASA Ames Research Center, Mountain View, CA. Instrument performance was verified by running the standard Ca-EDTA titration kit available from Malvern. All binding parameters for the test were within the specifications determined by the manufacturer and are included in the supplementary data.

To measure Cu binding (L, ligand) to our peptide (P), the ligand was prepared from cupric chloride, dihydrate, Crystal, BAKER ANALYZED™ A.C.S. Reagent, J.T. Baker™. Our peptides were synthesized by Elim Biopharmaceuticals (Hayward, CA and used without further purification. The protein solutions were prepared by dissolving a weighed amount of the lyophilized powder in 10 mM MES prepared from Alfa Aesar™ MES, 0.2 M buffer solution, pH 5.5 and the pH adjusted if needed with HCl (TraceMetal™ Grade.) Metal solutions were prepared by dissolving a weighed amount of the pure metal salts into the same stock MES buffer that was used to prepare the peptide solution to minimize the effect of the heat of dilution when measuring the samples. Both titrate and titrant solutions are de-gassed prior to loading into calorimeter cell and injection syringe.

The ITC experiments were run at 25°C and set to deliver 20-30, 0.5 – 1 µL injections at 150 second intervals. The procedure involved titrating $CuCl_2$ in excess to the cognate motif. Metal-chloride salts were chosen because they remain as dissolved ions. The experiments were run where the ligand solution in the syringe was added to the protein solution in the cell. Raw data were corrected for the heat of dilution. Integrated heat data were fit with a one-site binding model using the Origin-7™ software provided with the MicroCal iTC200. The ''best-fit'' parameters resulting from the nonlinear regression fit of these data are presented below.

Competition assays with competing ligands

E-waste components have different types and proportions of metals and these remain in solution after removal of the scaffold material. Fidelity of our chosen Cu-binding motifs

was assessed by adding metals with similar chemical properties such as Ni and Zn. These metals are competitors for the same ligand due to their similar electron configuration, ionic radius, valence, and/or binding affinity. In these experiments, a competing metal ion was added to the peptide-Cu complex or Cu was added to a metal-peptide complex. Intrinsic binding parameters were first determined for each peptide with individual metal ions, then binding parameters were obtained when a competing metal was titrated into the already-formed metal-peptide complex.

3.1.2.3 Results

The intrinsic and apparent binding parameters for selected peptides with cognate and competing metals are shown in Table IV.

Type	Name	Cu	Zn	Ni	Zn → Cu	Ni → Cu
Natural motifs	HypB1	2×10^6	-	-	2×10^6	2×10^6
	HypB2	2×10^6	-	-	2×10^6	2×10^6
	CZB-7	7×10^3	-	-	-	-
Consensus	Cu-02	4×10^4	-	-	-	-
Rational design	HHTC	4×10^6	2×10^3	-	7×10^5	7×10^5
	CHSK	1×10^6	-	-	2×10^5	2×10^5

Table IV. Intrinsic and apparent binding parameters for selected peptides

We began our ITC experiments with the rationally-designed peptide HHTC. It had been characterized previously with ITC, however the authors conducted experiments at pH 7 where thermodynamic modeling and experimental data reveal that Cu is mostly precipitated (>99%) into a solid mineral $Cu(OH)_2(s)$ phase at pH 7.[17] Thus, the observed binding parameters could be confounded by the change in enthalpy due to Cu dissociation from a solid mineral phase. We conducted our binding experiments at pH 5.5, where Cu is predicted to remain as Cu^{2+}. The published parameters for HHTC are: n = 1.01, $K_a = 2.4 \times 10^6$ [M^{-1}], ΔH = -28.5 kJ/mol, G_o = 36.4 kJ/mol. The parameters we obtained with HHTC and Cu at pH 5.5 were similar: n = 1, $K_a = 3.5 \times 10^6$ [M^{-1}], ΔH = -24.08 kJ/mol, G_o = 31.3 kJ/mol. The observed parameters for HHTC are within the $2\sigma = 1.4 \times 10^6$ despite having different experimental conditions with regards to buffer (prior

studies used ACES buffer) and pH. Previous research has found that there was no difference in intrinsic binding parameters for this peptide when using buffers with different heats of ionization, such as ACES and MES buffers, with ΔH_{ion} = 31.4 kJ/mol and 15.5 kJ/mol, respectively. This leads us to conclude that these are true binding parameters that accurately describe binding between Cu and the peptide under these conditions and not due to proton transfer or phase changes.

All peptides tested showed Cu binding with varied binding affinities. The binding parameters for all tested peptides are shown in the Table IV. The natural motifs HypB1, HypB2, and Czb7 have binding affinities ranging from high association constants K_a = 2 x 10^6 [M^{-1}] for HypB1 and HypB2, and K_a = 7 x 10^3 [M^{-1}] for Czb7. HypB1 and HypB2 have amino acid sequences: HypB1 Ac- CTT CGCG -NH2 and HypB2 Ac- MCTT CGCG EG -NH2 where the binding residues are identical with additional residues added to the N- and C- termini of the HypB2 peptide. The amino acid sequence for Czb7 is Ac- GFH GRA DAL LHKI -NH2 and it had a relatively low binding affinity of K_a = 7 x 10^3 [M^{-1}]. The consensus peptide Cu02 with amino acid sequence Ac- HCW CHM -NH2 had an intermediate binding affinity for Cu of K_a = 4 x 10^4.

These peptides were also assessed for their binding affinities to Zn and Ni, and none showed a binding isotherm when either Zn or Ni were titrated into the peptide. Additionally, competition experiments were conducted where the peptide with Zn and/or Ni are in solution and then Cu is titrated in. The resulting binding isotherms were identical to those where Cu was titrated in to the peptide with no other ions present. *This indicates that the peptides bind Cu only, and the affinity for Cu is not affected if there are Ni and/or Zn competing ions in solution.*

The results for our titration experiments with Cu and the rationally-designed peptides were comparable to the natural peptides. The peptide HHTC had a binding affinity for Cu of K_a = 4 x 10^6 [M^{-1}] and CHSK had a K_a = 1 x 10^6 [M^{-1}]. While there was no binding isotherm for the HHTC and CHSK when Ni or Zn were titrated in, the binding affinities for Cu were reduced by one order of magnitude when Ni or Zn were in solution. The association constant for HHTC-Cu was lowered from K_a = 4 x 10^6 →7 x 10^5 and 5 x 10^5 [M^{-1}] when Zn or Ni were in solution with the peptide, respectively. Similarly, CHSK-Cu binding affinity for Cu went from K_a = 1 x 10^6 → 2 x 10^5 [M^{-1}] when Zn was in solution.

3.1.2.4 Discussion

It was our goal to increase the TRL to at least 2 during Phase I grant period and we addressed several key unknowns that allow us to move forward in this project by testing the specificity of metal binding to engineered bacterial surfaces.

A recent review by has a thorough discussion about the principles of metal-peptide binding and only summarized here.[18] The review identified the determining factors that affect metal-ligand interactions as 1) metal coordination number (the ability to bind to a given number of ligands) and 2) molecular geometry between a ligand and its cognate metal. While these properties are important determinants for ligand specificity to a cognate metal,[19,20] we found that it is possible to bind metals efficiently and with specificity with only the consideration of the primary coordination sphere. Our results indicate that it is possible to use only the metal-binding amino acid partners in a protein motif to bind a cognate metal with specificity and high affinity. A query of the publicly available Protein Data Bank (http://www.rcsb.org/pdb/home/home.do) obtained the natural motifs, however there are many more metals in e-waste or of economic interest (rare-earth and platinum group elements) that have no role in biology, and thus no known protein partners. In these cases, we look to the peptides derived through rational design. This shows a promising approach in protein engineering because a cognate peptide for a specific metal can be designed, regardless of whether it has natural binding partners. The peptides derived *in silico* show comparable affinities and specificity to those found in nature.

3.1.3 Printing

Test the ability of the plasma jet system for in situ *tailoring of the deposited material properties using a simulated Martian atmosphere gas mixture.*

Increasing the TRL level of the concept has been the primary goal and it has been achieved by addressing several technical challenges including 1) controlled nebulizing of bioink for printing 2) precise substrate movement using an XY automated stage and 3) understanding the process parameters for efficient and reproducible printing of electronic materials.

Printing of electronic/optoelectronic devices using colloids faces numerous challenges with the major issue being oxidation of the material to be printed, leading to decreased mobility of the charge carriers. Copper has been of interest for various applications due to its high thermal and electrical conductivity, low cost and earth abundance. Nanostructured copper with varying oxidation states from pure metallic to cuprous oxide finds applications in printed electronics, optoelectronics and catalysis. Interconnects in

integrated circuits (IC) play a crucial role in deciding the system performance and speed. Printing of copper interconnects with controlled morphology and oxidation state is critical in 3D IC packaging, flexible printed circuit boards and vertical integration.

We used a dielectric barrier discharge (DBD) plasma jet system, where the plasma is ignited by applying a potential between two electrodes with He or Ar as the carrier gas passing through a quartz nozzle. The plasma is the most intense between the electrodes (active region) followed by the afterglow at the exit of the nozzle. Commercially available nozzles used here include Meinhard type C Quartz nebulizer with 0.5 mm capillary diameter and 5 mm diameter Pyrex Sheath Gas Tube (product id: ML116063). Nozzles are designed with two inlets. The inner capillary is used to inject the nanoparticles while the Larrier gas is introduced via the outer inlet. Copper tape wrapped around the glass nozzle acts as electrodes (3 cm apart) with one electrode ground and another connected to a high-voltage (1 to 15 kV) DC power supply. Scaling down the quartz nozzle allows a resolution of 120 microns and with precise control; achieving sub 100 μm resolution is possible. Figure 8(a) shows the plasma jet setup, Figure 8(b) shows a pattern printing using a high resolution nozzle on polycarbonate and Figures 8(c) and 8(d) show the SEM image of high resolution nozzles.

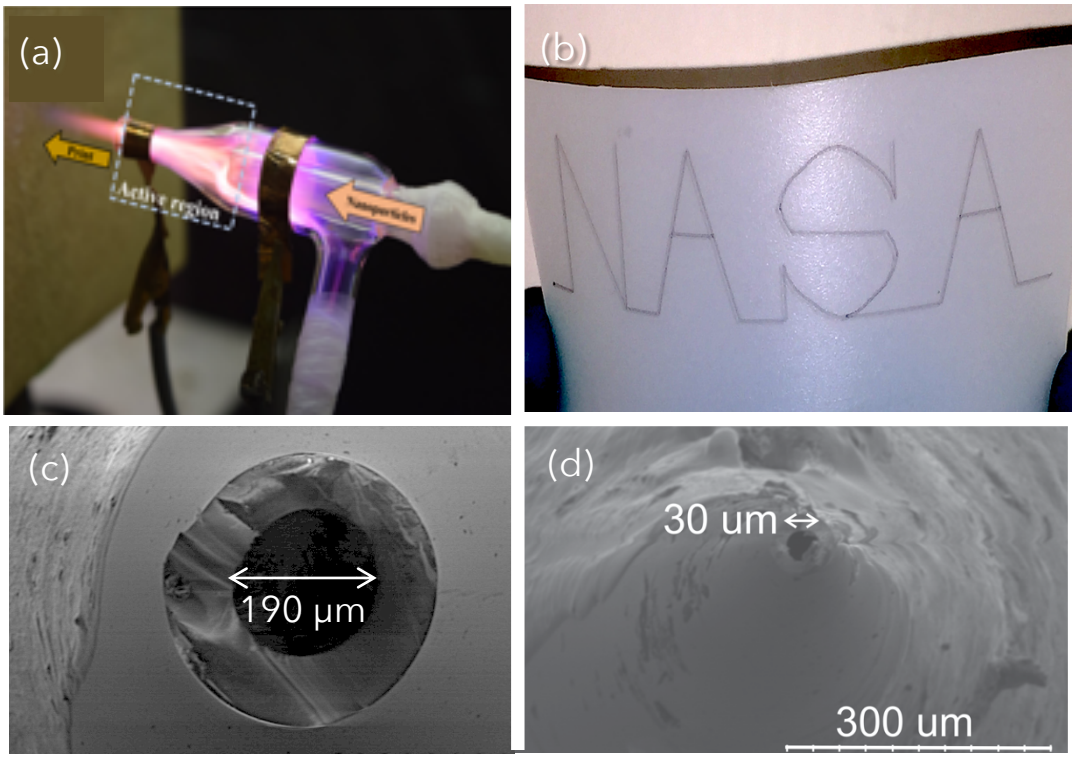

Figure 8.
Photographs of (a) plasma jet printing head (b) printing of copper on polycarbonate (c) SEM image of nozzle with 190 μm diameter and (d) SEM image of nozzle with 30 μm diameter

Print the new bioinks using the plasma jet system and test the ability of the plasma jet system for in situ *tailoring of material properties*

The metal in the aerosol, upon entering the region in the nozzle containing the plasma, is subjected to combined electrical and magnetic fields, electro-hydrodynamic forces, and bombardment by plasma species. Additionally, there are thermal and chemical phenomenon that affect the thermal conductivity of the gases due to molecular excitation, de-excitation and collisions in the plasma. The plasma jet properties can be exploited to create directionality and this allows for printing in a micro-gravity environment.

The momentum the plasma particles carry during collisions with a substrate serve to form a coating that varies depending on different factors including; gas flow ratio, nature and type of gases, applied voltage, size and shape of the nozzle, distance between the substrate and plasma jet, etc. This will affect both the morphology and chemical structure of the material being deposited. By carefully controlling the gas mixtures and process parameters, it is possible to control the morphology, porosity and surface roughness of the deposited film. The material properties can be tailored in one or more of the following states; a) while in the aerosol prior to deposition, b) on the substrate during deposition, and/or c) on the substrate post deposition.

The gases in the Martian atmosphere can be used to process the biomined ink, and we will conduct simulations with these gas mixtures. Subsequently, we will characterize the oxidation state and the local electronic structure of the printed structures using x ray absorption spectroscopy at SLAC National Accelerator Laboratory.

Plasma jet printing of conductive patterns with bioinks were conducted with argon as a primary source gas and a nitrogen/hydrogen mixture as the reactive gases. *The presence of the reactive gases removed the hydrocarbons in the bioink and the plasma process parameters were optimized to tailor the oxidation state and the electronic structure of the copper interconnects.* The current and voltage requirements for the plasma jet were measured using an IV probe for additional optimization and characterization of our procedures. In addition to silicon wafers, flexible substrates and non-conformal 3D objects were used as substrates for printing.

We have successfully optimized the plasma printing process for printing copper from biomined ink. As the printing of biomined ink will result in organic contaminations, it is absolutely necessary to remove the organics and print the required metallic structure. The biomined ink containing copper was printing using various process gases and the composition was analyzed using energy dispersive analysis by x ray spectroscopy (EDS). As shown in Figure 9, the deposited ink (without plasma) shows a range of organics and the removal of organic contaminants is evident when the argon and hydrogen gas mixtures were used. The solid copper oxide nanoparticles can be transformed to a metastable state of solid liquid phase by varying the process parameters in which the surface transforms to liquid while the bulk remains solid. This will have an impact on both the morphology and chemical structure of the material being deposited. This partial molten outer core of the nanoparticles also aids in better adhesion to the substrate.

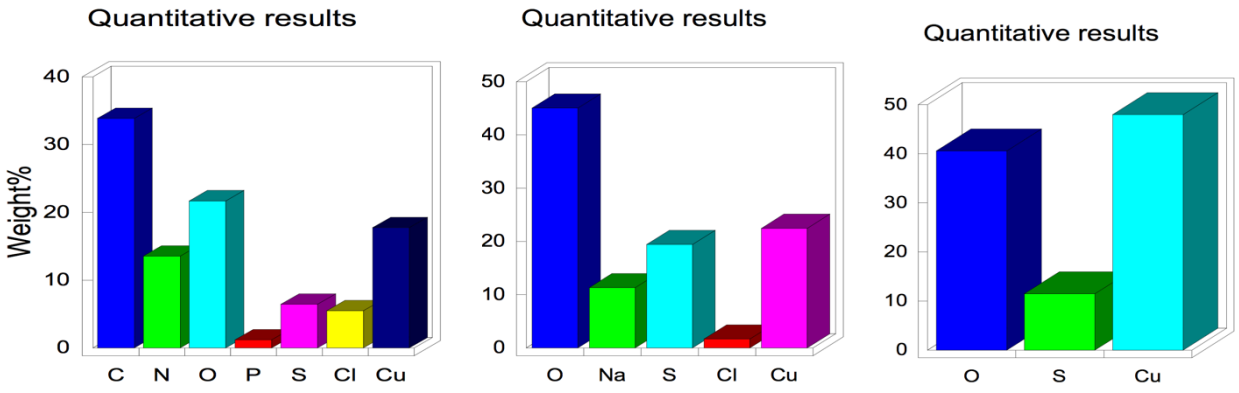

Figure 9. *Elemental composition measurement using EDS on biomined ink printed (left) without plasma, (middle) with argon plasma (right) with argon+hydrogen mixed plasma*

Further, direct write plasma printing of copper thin film with tailored oxidation state is demonstrated and characterized using x ray absorption spectroscopy and electrical measurements.

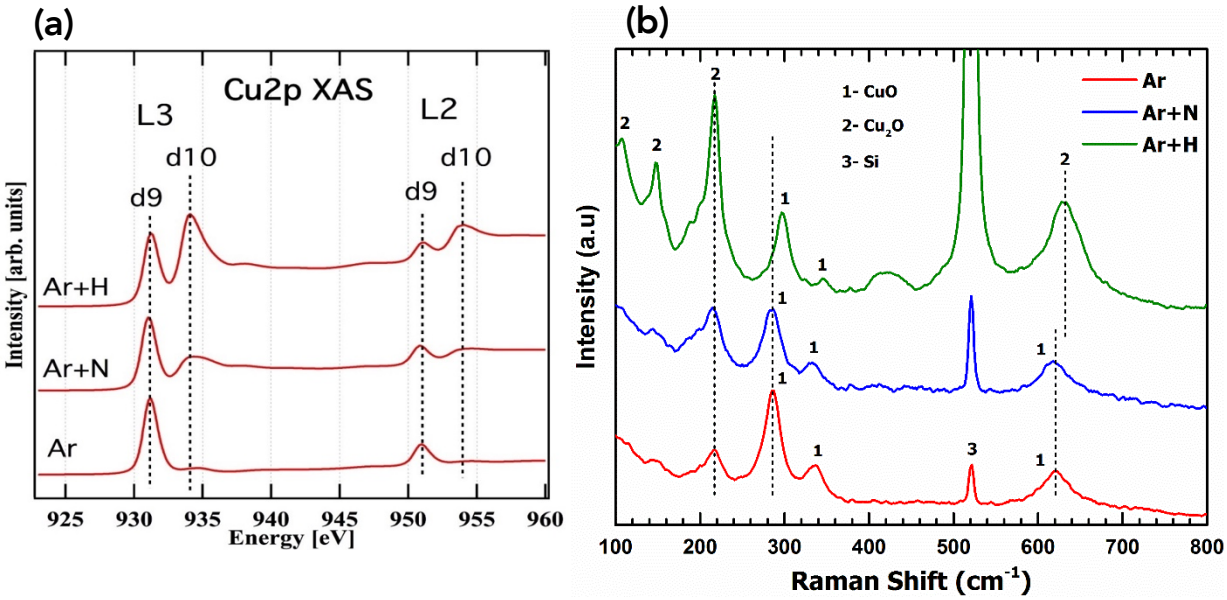

Figure 10. *(a) Cu $L_{2,3}$-edge and O K-edge XAS spectra of printed copper films in total electron yield (TEY) mode. (b) Raman Spectra of the printed copper films.*

X-ray absorption spectroscopy (XAS) was performed to gain an insight into the electronic state of the printed copper films as shown in Figure10a. XAS has been widely used to probe into density of unoccupied states of various materials. It is highly sensitive towards changes in electronic state or chemical environment of an atom. The electronic configurations for the states Cu^0, Cu^{1+} (cuprous oxide), Cu^{2+} (cupric oxide) were observed for various process conditions. Regardless of the presence of surface contaminants, the variation in absorption of copper core level is evident for tuning of oxidation state of plasma printed copper film. The current-voltage characteristics of the samples are also studied as shown in Figure 10b. For comparison, copper colloidal solution was drop-casted and also deposited aerosolized nanoparticles (without turning on the plasma) on silicon wafer. Both these samples showed very low conductivity and their resistance values were in the range of ~ 100 MΩ. The drop-casted sample showed enhanced conductivity when post-treated with plasma jet for just 1 min, the conductivity of this sample was higher than a four-hour annealed sample, where the annealing was carried out in a tube furnace at 500 °C in Ar/H_2 atmosphere. *This is an indication of the advantage plasma jet processing offers over standard temperature-dependent*

techniques. When the same nanoparticle colloid was printed using Ar/H plasma, it showed a significant rise in conductivity which is indicative of the fact that *in situ* process can be used to create conductive patterns from a rather insulating ink. When the printing process was extended with the flow of nanoparticles being cut off, the printed samples showed a drastic drop in resistance.

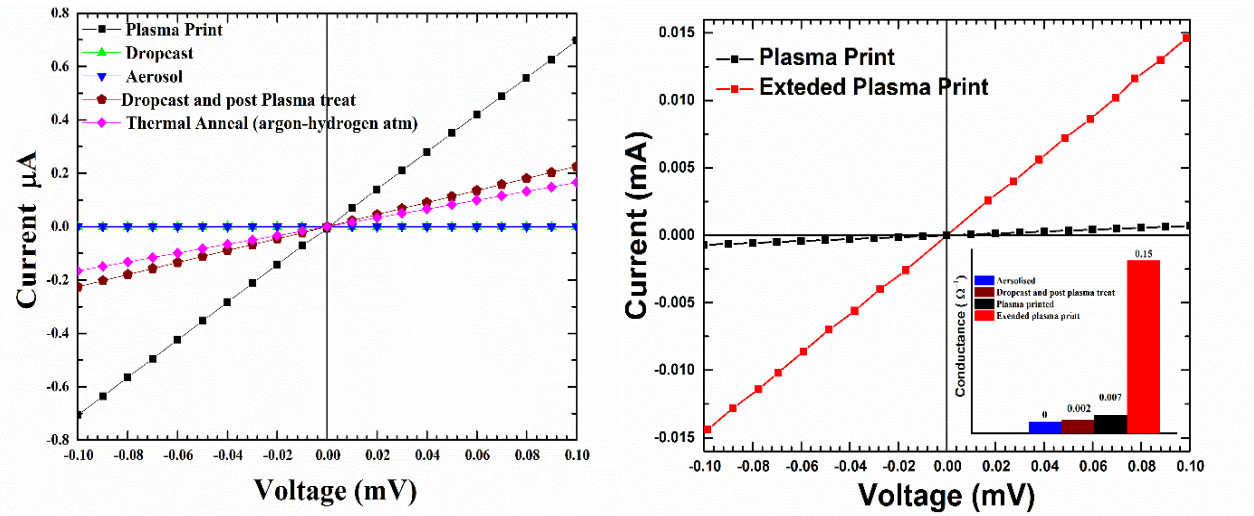

Figure 11. *I-V characteristics of the printed copper film (a) under various process conditions and (b) printing and extended plasma printing*

The current-voltage characteristics of the samples are shown in Figure 11. For comparison, copper colloidal solution was drop-casted and also deposited aerosolized nanoparticles (without turning on the plasma) on silicon wafer. Both these samples showed very low conductivity and their resistance values were in the range of ~ 100 MΩ. The drop-casted sample showed enhanced conductivity when post-treated with plasma jet for just 1 min, the conductivity of this sample was higher than a four-hour annealed sample, where the annealing was carried out in a tube furnace at 500 °C in Ar/H_2 atmosphere. This is an indication of the advantage plasma jet processing offers over standard temperature dependent techniques. Plasma exposure resulted in partial melting of the nanoparticles creating electrical pathways and hence improving the conductivity. Collision of the high temperature electrons with nanoparticles must have created local hot spots. Also, the high energy free electrons and ions may have partially reduced CuO to metallic copper and the momentum they carry may have deformed the nanoparticles. Evident from these results, electron and ion temperature play a crucial role in defining the electronic properties of printed material in addition to gas

temperature. The presence of energetic vacuum ultraviolet radiation at the effluent of the plasma jet cannot be negated as well.

When the same nanoparticle colloid was printed using Ar/H plasma, it showed a significant rise in conductivity. Although the resistance is of the order of 150 Ω, but the rise in conductivity is indicative of the fact that *in situ* process can be used to create conductive patterns from a rather insulating ink. When the printing process was extended with the flow of nanoparticles being cut off, the printed samples showed a drastic drop in resistance. The steep rise in conductance is shown in Figure 11 (b) inset. Thus, exposing the sample with the same plasma jet resulted in ~20 times decrease in resistance value (7 Ω). The increased concentration of metallic copper may be the principle cause of this phenomenon, which is in line with the XAS observation. One may argue on using other non-plasma printing processes and rather use the plasma jet for a post treatment of the samples for improved conductivity. But the formation of conductive interconnects within the films will be hard to achieve. Figures 5a and 5b inset show I-V curve and conductance of copper samples drop-casted and post treated using plasma jet. It is evident that the conductance of the plasma prints and post-treated samples are 80-100X than that of the drop-casted and post-treated sample. Although the conductance values were quite high for "as synthesized" samples, these samples showed a considerable deterioration in conductance values over time. This is mainly due to the surface oxidation of the copper nanoparticles when subjected to ambient conditions. The measured conductance values averaged over three different samples was found to be 14 S/m after a 30-day ambient exposure. However, after exposure to intense pulse light (3kV, 1 pulse) the same samples showed a four order of magnitude increase in conductivity ($3.42 * 10^5$ S/m). In spite of this noticeable increase, this value is considerably lower than that of bulk copper (10^8).

Figure 12 shows SEM images of copper nanoparticle film printed using different plasma conditions. Nanoparticles printed with a He plasma (@ 1600 sccm) retain their shape and do not undergo any physical deformation to a significant extent, as evident in Figures 12 (a, b). The particles are agglomerated but are mostly spherical similar to the as-synthesized nanoparticles. Figure 12 (c, d) shows copper nanoparticles deposited using an Ar plasma. As the ion density and gas temperature is higher in this case, the nanoparticles undergo physical deformation resulting in uniform film formation. The gas temperature of Ar plasma is sufficiently high to partially melt the nanoparticles. This fluidic nanospheres, after reaching the substrate, tend to aggregate to reduce the surface energy forming a thin film. When nitrogen is introduced into the helium plasma,

the electron density, electron temperature and the current density increase. As shown in Figures 12 (e, f), the smaller particles undergo partial physical deformation while the larger nanoparticles retain the shape to a certain extent resulting in film formation with particles embedded on it.

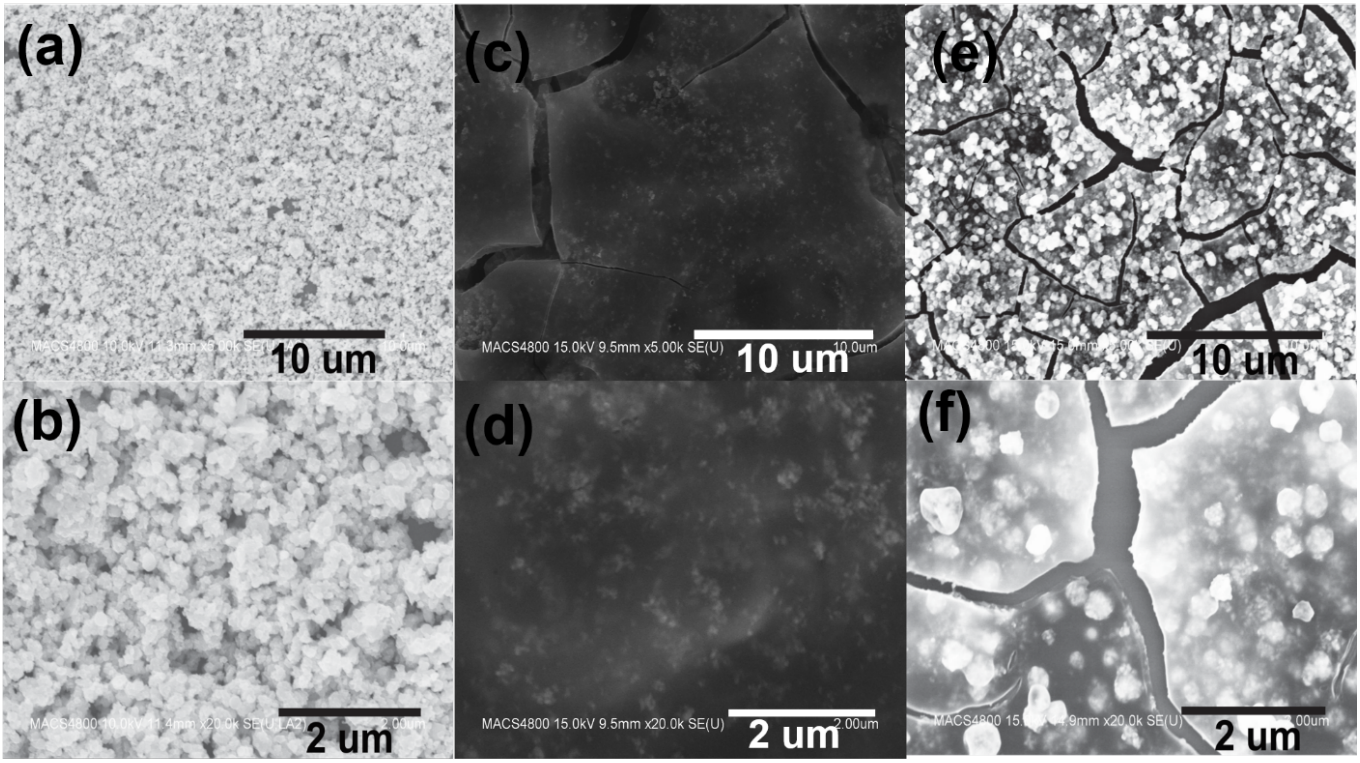

Figure 12. *SEM images of printed copper nanoparticles a,b) with He Plasma c,d) with Ar plasma e,f) Plasma with He and N in 4:1 ratio.*

The I-V and XAS measurements confirm that a highly conductive pattern can be printed from a rather insulating oxide ink. This system also promotes adhesion to the substrate, uniformity in deposition and formation of densely packed nanoparticle structure. By varying the gases in the plasma, a desired morphology and electronic structure can also be achieved.

Printed Antenna

To demonstrate a functioning electronic device, an RF antenna was printed that could potentially be used for communication. This demonstration extends the applicability of the plasma jet printing for a range of electronic devices including integrated circuits, antenna and communication devices.

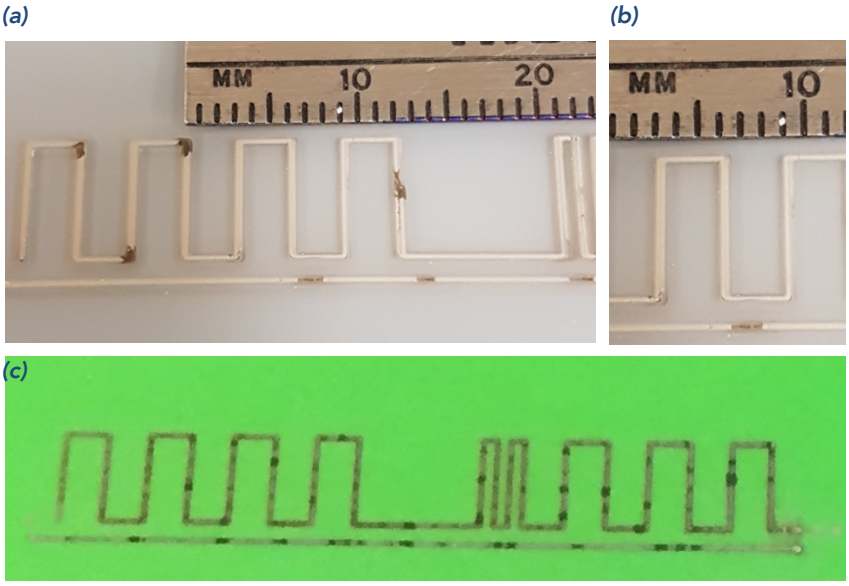

Figure 13. *(a) and (b) Photographs of silver antenna printed on flexible polycarbonate substrates and (c) Photograph of silver antenna printed on flexible cellulose substrate.*

Figure 13 shows silver antenna printed using plasma jet process on flexible polycarbonate and cellulose substrates. In order to print materials on a range of substrates including semiconductor wafers, textiles, paper, plastics and other flexible substrates, advanced manufacturing technologies are essential. The plasma jet deposition technique presented here offers unique capability to deposit metals and metal oxides with tailored physical and chemical characteristics. By varying the gases in the plasma, a desired morphology and electronic structures has been achieved. The results affirm plasma jet printing as a promising technology for manufacturing of next-generation printed electronics products.

3.2 Objective 2. Analysis of influence of technology on mission architecture

The problem.

Electronic devices are especially susceptible to radiation induced damage, often causing device failure. For example, recent solar events caused instrumentation failure in the form of memory errors in the Mars Odyssey mission. Such a failure could be catastrophic on a future human mission. In addition to solar events, long-duration cumulative ionizing doses also can cause degradation and damage to electronic components. Electronic repair and replacement strategies will be required for long duration and habitation missions, where resupply is challenging or not viable. As evidenced from the initiation of the Component-Level Repair During Spaceflight (CLEAR) project, NASA has acknowledged the need for electronics fabrication and repair capabilities to reduce mission risk and costly resupply for long duration spaceflight.[21] To date, the CLEAR project has performed the Component Repair Experiment-1 on ISS to evaluate electronic component-level repair, in particular removing nonfunctional components and soldering new components.[22] The NASA CLEAR project is a step in the right direction

but will still require batches of component parts to make repairs. In this proposed project, we look to a solution where all components can be generated in space.

The sources of these degradation and failures are divided into total ionizing dose effects, displacement damage and single event effects. Electronics are susceptible to damage from particles ranging from 10s of MeV as from trapped electrons to TeV in the case of galactic cosmic rays.[23] Examples of anomalies to component failures caused by space radiation exist within NASA's history.[24]

Human spaceflight is currently constrained to the International Space Station (ISS). Electronics on the ISS are comprised of modular units called orbital replacement units (ORUs). NASA's approach has been to make efficient maintenance of electronics on ISS by the following: 1) trace the fault to a specific ORU and 2) replace the ORU with a backup. While the replacement of ORU's has minimized crew time to repair faulty electronics, it has resulted in high payload costs and has required constant resupply to ISS. ORUs are comprised of many individual components. When one component goes bad, the entire ORU is replaced. To minimize payload costs, component level failures should be addressed and repaired or replaced at the component level. And as humans explore further from the Earth, resupply of backup ORUs is just not an option. The Component-Level Electronic-Assembly Repair (CLEAR) project out of NASA GRC has studied the need for tooling to repair component level electronic failures.[25]

Mission

As outlined in the document NASA's Journey to Mars: Pioneering Next Steps in Space Exploration, NASA is preparing a human mission to Mars. But unlike our prior human missions to Moon, this time our goal is to stay on Mars.[26] In such a mission, it is anticipated that use of *in situ* resources utilization (ISRU) technologies will be significant. This study broke such ISRU technologies into two campaigns, a light ISRU campaign and an extensive ISRU campaign. In the extensive ISRU campaign, plastics may be built using methane manufactured on Mars. The plastic can be fed into a 3D printer to manufacture spare parts on demand.[27] In this proposal, we identify additional ISRU and printing technologies that can be used to manufacture electronics on demand.

Long-duration sustained operation of electronics is challenging enough that an ISRU approach to manufacture and/or repair electronics is of value. The Human Exploration of Mars Design Reference Architecture 5.0, electronic components face potential damage due to ionizing radiation effects and electrified dust.[28] Electronic components brought to Mars for long-duration robotic missions and eventual human habitation on

Mars will face challenges in shortened operational shelf-life due to harsh radiation and dust storms effects of the Mars environment. This combined with limited resources and expense of resupply missions, there is significant need to develop ISRU technologies to enable the repair and manufacturing of electronic components on Mars. We propose infusion of our NIAC technology into future human exploration and habitation of Mars through first a demonstration of critical technologies in the actual Martian environment, Objective B in the MEPAG Goal IV: prepare for human exploration. Objective B calls to conduct risk and/or cost reduction technology and infrastructure demonstrations in transit to, at, or on the surface of Mars.[29]

Printing vs Resupply

With typical launch costs to lower earth orbit ranging from $4,640/kg on a Falcon 9 to $20,200/kg on Atlas V, there is great financial gain if we develop a strategy to harvest, recycle and reuse supplies. Now when one considers a trip beyond lower earth orbit, like one to Mars, the cost will hinder resupply. Under the Extensive ISRU campaign outlined, Mars explorers would only receive supplies from two SLS launches per year, necessitating either significant redundancy of electronics and/or an ISRU approached to manufacture on the Martian surface.[29] We envision that an electronic materials printer could integrate with the plastic 3D printer and could draw from the same 5 kW of power.

Printed electronics is a field that is currently gaining much momentum, with an estimated market value of $200 billion.[30,31] Leading examples are in the areas of photovoltaics, flexible batteries, electro-optic devices, displays, logic and memory devices, sensor arrays, RFID tags.[32] Of the variety of printing techniques commonly employed to manufacture printed electronics, inkjet and aerosol jet are two of the most common. In inkjet, a colloidal suspension of nanomaterial based ink is dropped out of a small pinhead nozzle. Common printers such as the Dimatix materials printer use a piezo drop on demand method for pushing ink out the printer nozzle. The most commonly encountered problem with this style of printer is nozzle clogging. Aerosol jet eliminates the problem of clogging by aerosolizing the nanomaterial ink and pushing it out a small nozzle with an inert carrier gas. However, problems with ink adhesion commonly occur. Our printer technology uses aerosolized nanomaterials but with the addition of an atmospheric pressure plasma of tunable chemical composition (see section 3.1.3). The plasma helps the nanomaterial stick to the support substrates and the tunable composition of the plasma is used to chemically modify the ink as it's being deposited.

Printed electronics aren't able to obtain the same feature sizes as those produced in a cleanroom here on earth. For example, resolution of typical inkjet printers are ~20 μm, whereas Intel's CMOS process has produced down to 14 nm technology.[33] Typically, smaller size is attributed to lowering production costs, because more components can fit onto one silicon wafer in the fabrication process. Since production cost is not a major concern to a human pioneering Mars mission, the substantially larger feature size is not a concern.

3.3 Objective 3. Analysis of impact of this technology on terrestrial applications

Integrating electronics printing with 3D printing is an unmet need in additive manufacturing with large market potential. Plasma printing can enable new products like 3D printed objects with embedded electronics, wearable monitoring devices, batteries, etc. With the rapid growth of the flexible electronics industry on Earth, there is a need for advanced printing technologies for embedding electronics on non-traditional platforms such as plastics, paper, and textiles. This will enable new features such as printing of antennas, sensors, signal circuitry, catalytic deposition, etc. This technology offers a competitive advantage over other state-of-the-art printers that use inkjet, aerosol and screen printing.

Our biomining technology can affect the current situation on Earth with end-of-life electronics, so called e-waste. There is currently no technology or infrastructure in place in the United States to reclaim these valuable metals. We assessed the financial, health and environmental costs of current recycling technologies as this has become an issue of global concern that has spurred legislation development to restrict e-waste exports to developing countries (Responsible Electronics Recycling Act – HR 2284) due to deleterious effects on the environment and human health. Technological advances and breakthroughs have accelerated the rate at which consumer electronics are expended, as older technologies are phased out and electronics become obsolete. These advances, along with the lack of strategies to implement recycling or disposal have led to fragmented approaches for dealing with e-waste. The glass and metals in e-waste components can be reused or recycled; however developed countries tend to not recycle due to high labor costs and strict environmental regulation. Instead, e-waste accumulates in landfills or is exported to developing countries where it is recycled using primitive techniques (*i.e.*, open air incineration, acid treatment) without regard for worker safety or environmental impact.[34] Many components in e-waste contain limited geological resources such as platinum group, transition, and precious metals such as Pt,

Cu and Au, respectively. Our analysis will elucidate how this biotechnology can lead to the development of infrastructure that can have minimal environmental impact. The only way to deal with the growing problem of e-waste is to make it economically viable. If we can develop the technology to lower the cost and efficiency of recycling e-waste, then it would compete with the cut-rate prices of raw materials. Once the technology has been developed, a systematic and regulated infrastructure can be established in the communities that have economies based on e-waste; a new way of dealing with a global issue.

Biomining vs Electrodeposition

Mars, like Earth, has valuable mineral deposits that can be mined to produce a multitude of useful products including metals for electronics, Figure 14.[35,36] In addition, the metals from spent electronics can also be reharvested to expand the breadth of electronic materials. Extraction metallurgy is characterized by three consecutive processes 1) leaching 2) concentration and 3) pure metal recovery.

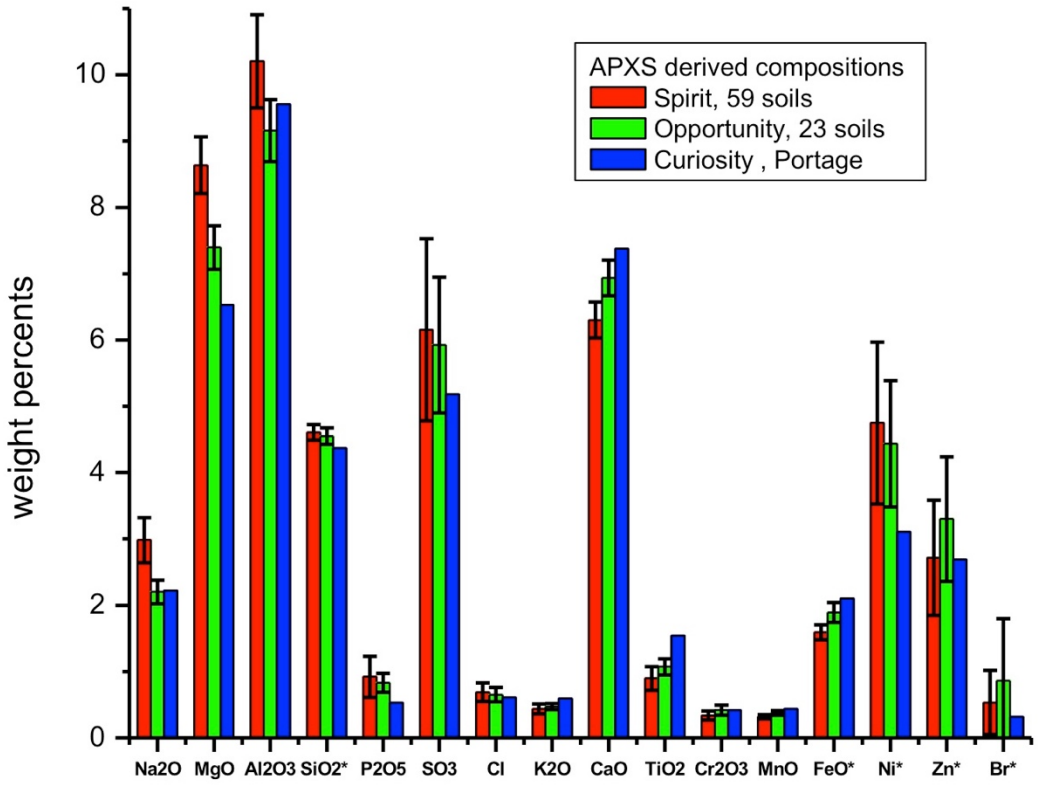

Figure 14. Comparison of soil analysis by Mars Rovers Spirit, Opportunity and Curiosity as measured by alpha particle x-ray spectroscopy (APXS).[29]

Leaching is a process typically performed by a using concentrated acids to dissolve metal ions from mineral sources and is typically referred to as chemical leaching. Bioleaching is performed by microorganisms that specifically bind metals and metal oxides and is becoming an attractive alternative to chemical leaching due as a way to avoid large amounts of chemical waste products. A study by Bayat and colleagues[37] compared chemical and microbial leaching processes against Zn, Cu, Ni, Pb, Cd and Cr. While chemical leaching efficiencies were found to be 79% Zn, 75% Cu, 73% Ni, 70% Pb, 65% Cd and 22% Cr, microbial leaching efficiencies were higher, 97% Zn, 96% Cu, 84% Pb, 67% Cd, 34% Cr. While bioleaching is efficient, it is a slower process, typically ~20 days for microbial leaching vs ~4 days for chemical leaching. Both processes were carried out at pH 2 with H_2SO_4 and at 25°C. However, bioleaching is chemically cleaner with fewer waste products. Our proposed biomining method is even less toxic as should be carried out at ambient temperatures and a neutral pH in a non-toxic culture medium.

Metal	Chemical Leaching Efficiency	Microbial Leaching Efficiency	Chemical Leaching Rate Constant k (day^{-1})	Microbial Leaching Rate Constant k (day^{-1})
Zn	79%	97%	0.0168	0.1734
Cu	75%	96%	0.0209	0.1762
Ni	73%	93%	0.0204	0.1267
Pb	70%	84%	0.0174	0.0832
Cd	65%	67%	0.0147	0.0595
Cr	22%	34%	0.0036	0.0214

Table V. Efficiency of different metal recovery methods.[37]

The second step of extraction metallurgy is concentration. This is a process of chemical extraction used to separate contaminates from metal ions. By using microorganisms instead of concentrated acids, the process of concentration is reagent neutral and becomes one of microbial concentration, using a centrifuge instead of

chemicals. Metal recovery is typically performed by electrolysis. This process uses an electrochemical cell to plate very pure metal at one electrode. In this NIAC project, we propose to eliminate this step entirely. By printing the microorganism with metal ion directly through the atmospheric pressure plasma, we ash the carbon from the microorganism and print just the metal. By tuning the atmosphere of the plasma to a reducing environment, as with the addition of H_2 gas, we reduce the metal oxides to pure metals as they are printed into circuits. Clearly the process of microbial leaching followed by plasma printing eliminates concentrated chemical waste products. That being said, electroplating is not inconsistent with biomining as a final step.

4. The Team

From phase I proposal:

The worked together under an FY15 AES award, and is tightly integrated and co-located in building N239 at NASA Ames Research Center

Lynn Rothschild (PI), is a pioneer in the use of synthetic biology for space applications, as well as a leader in the field of astrobiology. As PI she oversaw the project, supervised the bioengineering which took place in her lab at Ames, and contributed to this final report.

Jessica Koehne (Co-I), has been developing nanomaterial-based sensors and electronics for NASA since 2001. She currently leads a group in sensor development and printable electronics. She oversaw the printing work, and lead Objective 2, impact on mission architecture.

Ram Gandhiraman (Co-I), a research scientist with USRA at NASA, is a 2007 Ph.D. with strong expertise in Materials Science and Engineering. He is the lead inventor of atmospheric pressure plasma jet printing technology (US patent: 14/515,072). His focus was on printing and *in situ* tailoring of material properties using martian atmospheric gas mixture, miniaturizing the printing system for flight test, and helping with Objective 2, impact on mission architecture.

Jesica Navarrete (graduate student), is a PhD candidate in the Microbiology and Environmental Toxicology Department at The University of California, Santa Cruz. Her undergraduate training was in microbiology and chemistry, while her M.S. is in geochemistry. She performed the biomining work and contribute to Objective 3, Analysis of impact of this technology on terrestrial applications as part of her Ph.D.

thesis, and Objective 2 when geology expertise is needed. She is also doing the day-to-day supervision of Dylan Spangle.

At the end of the project (January 2017) we were able to add a masters student in BioEngineering from Brown University, **Dylan Spangle**, to focus on the silicase work for his thesis. The silicase work presented here is the first part of his thesis to be presented in April 2017.

5. References

[1] Madou, M. J. 1997. *Fundamentals of Microfabrication* (CRC, Boca Ranton, FL).

[2] Gandhiraman, R.P., Jayan, V., Meyyappan, M. & Koehne, J. Atmospheric pressure plasma based fabrication of printable electronics and functional Coatings. US Patent application 14/515,07

[3] Gandhiraman, R.P., Jayan, V., Han, J-W., Chen, B., Jesica Koehne, J. & Meyyappan, M. 2014. Plasma Jet Printing of Electronic Materials on Flexible and Non-Conformal Objects. *ACS Appl Matter Interfaces*. **6**, 20860.

[4] Horneck, G., Bucker, H., Reitz, G., 1994. Long-term survival of bacterial spores in space. *Adv. Space Res.* **14**: 41–5.

[5] Horneck, G., Klaus, D.M. & Mancinelli, R.L. 2010. Space Microbiology. *Microbiology and Molecular Biology Reviews*, **74**: 121-56.

[6] Moravej, M., Yang, X., Nowling, G.R., Chang, J.P., Hicks, R.F. & Babayan, S.E. 2004. Physics of high-pressure helium and argon radio-frequency plasmas. *J. Appl. Phys.* **96**: 7011.

[7] Fu, C., Olson, J.W. & Maier, R.J. 1995. HypB protein of *Bradyrhyzobium japoicum* is a metal-binding GTPase capable of binding 18 divalent nickel ions per dimer. *PNAS* **92**: 2333-7.

[8] Chung, K.C.C., Cao, L., Dias, A.V., Pickering, I.J., George, G.N. & Zamble, D.B. 2008. A high-affinity metal-binding peptide from *Escherichia coli* HypB. *JACS* **130**: 14056-7.

[9] Yeh, K. & Kung, C.S. 2010. Metal-binding motif compositions and methods. United States Patent No: 7,659,362

[10] Bertini, I., Cavallaroa, G. & McGreevya, K.S. 2010. Cellular copper management - a draft user's guide. *Coordination Chemistry Reviews* **254**: 506–24.

[11] Kosizek, M., Svato, A., Budesinsky, M., Muck, A., Bauer, M.C., Kotrba, P. & Rulizek, L. 2008. Molecular Design of Specific Metal-Binding Peptide Sequences from Protein Fragments: Theory and Experiment. *Chemistry-A European Journal* **14(26):** 7836-46.

[12] Wang, F. & Sayre, L. M. 1989. Oxidation of tertiary amine buffers by copper(II). *Inorg. Chem.* **28 (2**): 169–70.

[13] Kandegedara, A. & Rorabacher, D. B. 1999. Noncomplexing Tertiary Amines as "Better" Buffers Covering the Range of pH 3−11. Temperature Dependence of Their Acid Dissociation Constants. *Anal. Chem.* **71 (15):** 3140–4.

[14] Gustafsson J. P. 2007. Visual MINTEQ, version 3.0. Available from: http://vminteq.lwr.kth.se/download/ .

[15] Nielsen, A. D., Fuglsang, C. C. & Westh, P. 2003. Isothermal titration calorimetric procedure to determine protein–metal ion binding parameters in the presence of excess metal ion or chelator. *Analytical Biochemistry* **314(2):** 227-34.

[16] Wilcox, D. E. 2008. Isothermal titration calorimetry of metal ions binding to proteins: An overview of recent studies. *Inorganica Chimica Acta* **361**: 857–67.

[17] Navarrete, J.U., Borrok, D. M., Viveros, M., Ellzey, J.T. 2011. Copper isotope fractionation during surface adsorption and intracellular incorporation by bacteria. Geochimica et Cosmochimica Acta. 75, 784-799.

[18] Dudev, T. and Lim, C. 2014. Competition among metal ions for protein binding sites: Determinants of metal ion selectivity in proteins. *Chemical Reviews* **114**: 538-56.

[19] Benson, D.E., Wisz, M.S., Liu, W. & Hellinga, H.W. 1998. Construction of a novel redox protein by rational design: Conversion of a disulfide bridge into a mononuclear iron-sulfur center. *Biochemistry*. **37**:7070-6.

[20] Yang., W., Jones, L.M., Isley, L., Ye, Y., Lee, H.W., Wilkins, A., Liu, Z., Hellinga, H.W., Malchow., R., Ghazi., M. & Yang., J.J. 2003. Rational design of a calcium-binding protein. *JACS* **125**: 6165-71.

[21] Pettegrew, R. D., Easton, J., Struk, P. "Repair of Electronics for Long Duration Spaceflight" *45th AIAA Aerospace Sciences Conference* 8-11 Jan. 2007; Reno, NV; United States

[22] Easton, J. W., Struk, P. M. "Component Repair Experiment-1: An Experiment Evaluating Electronic Component-Level Repair During Spaceflight" *NASA/TM-2012-217022*.

[23] Barth, J. L. et al., 2003. *IEEE Transaction on Nuclear Science*, 50.

[24] Leach, R. D. & Alexander, M. B. 1995. NASA Reference Publication 1374.

[25] Oeftering, R. C., Wade, R. P. & Izadnegahdar, A. 2011. Component-Level Electronic-Assembly Repair (CLEAR) Spacecraft Circuit Diagnostic by Analog and Complex Signature Analysis, NASA/TM-2011-216952.

[26] [4]NASA's Journey to Mars: Pioneering Next Steps in Space Exploration, https://www.nasa.gov/sites/default/files/atoms/files/journey-to-mars-next-steps-20151008_508.pdf, accessed Jan 1, 2017.

[27] Arney, D. C., Jones, C. A., Klovstad, J. J., Komar, D. R., Earle, K., Moses, R., & Shyface H. R. 2015. "Sustaining Human Presence on Mars Using ISRU and a Reusable Lander." *AIAA Space 2015 Conference and Exposition*, 2015, AIAA 2015-4470).

[28] Drake, B. G., et al., 2009. *Human Exploration of Mars Design Reference Architecture 5.0*, NASA-SP-2009-566

[29] Grant, J., et al., 2006. "Mars Science Goals, Objectives, Investigations, and Priorities: 2006", Mars Exploration Program Analysis Group (MEPAG).

[30] Kantola, V., Kulovesi, J., Lahti, L., Lin, R., Zavodchikova, M. & Coatanea, E. 2009. "Printed Electronics, Now and Future" Bit Bang: Rays to the Future, ed. Neuvo, Y., Ylonen, S. Helsinki University Print.

[31] Perelaer, J., Smith, P. J., Mager, D., Soltman, D., Volkman, S. K., Subramanian, V., Korvink, J. G. & Schubert, U. S. 2010. *Journal of Materials Chemistry* **20**: 8446-53.

[32] Khan, S., Lorenzelli, L. & Dahiya, R. S. 2015. *IEEE Sensors Journal* ***15***: 3164-85.

[33] http://www.intel.com/content/www/us/en/silicon-innovations/intel-14nm-technology.html, accessed Jan 1, 2017.

[34] Cobbing, M. (2008). *Toxic Tech: Not in Our Backyard. Uncovering the Hidden Flows of e-waste. Report from Greenpeace International.* http://www.greenpeace.org/raw/content/belgium/fr/press/reports/toxic-tech.pdf, Amsterdam.

[35] http://mars.jpl.nasa.gov/msl/multimedia/images/?ImageID=4910, accessed Jan 1, 2017.

[36] Kieffer, H. H. 1992. *Mars*. University of Arizona Press.

[37] Bayat, B. & Sari, B. 2009. Comparative evaluation of microbial and chemical leaching processes for heavy metal removal from dewatered metal plating sludge. *J. Hazard Mater*ials **174:** 763-9.